ACS POLYMERS Au
AN OPEN ACCESS JOURNAL OF THE AMERICAN CHEMICAL SOCIETY

pubs.acs.org/polymerau
Article

All-Polymer Nanocomposite as Salt-Free Solid Electrolyte for Lithium Metal Batteries

Jorge L. Olmedo-Martínez, Rafael Del Olmo, Antonela Gallastegui, Irune Villaluenga, Maria Forsyth, Alejandro J. Müller,* and David Mecerreyes*

Cite This: ACS Polym. Au 2024, 4, 77−85
Read Online
ACCESS | Metrics & More | Article Recommendations | Supporting Information

ABSTRACT: Solid polymer electrolytes that combine both a high lithium-ion transference number and mechanical properties at high temperatures are searched for improving the performance of batteries. Here, we show a salt-free all-polymer nanocomposite solid electrolyte for lithium metal batteries that improves the mechanical properties and shows a high lithium-ion transference number. For this purpose, lithium sulfonamide-functionalized poly(methyl methacrylate) nanoparticles (LiNPs) of very small size (20−30 nm) were mixed with poly(ethylene oxide) (PEO). The morphology of all-polymer nanocomposites was first investigated by transmission electron microscopy (TEM), showing a good distribution of nanoparticles (NPs) even at high contents (50 LiNP wt %). The crystallinity of PEO was investigated in detail and decreased with the increasing concentration of LiNPs. The highest ionic conductivity value for the PEO 50 wt % LiNP nanocomposite at 80 °C is 1.1 × 10^{-5} S cm^{-1}, showing a lithium-ion transference number of 0.68. Using dynamic mechanic thermal analysis (DMTA), it was shown that LiNPs strengthen PEO, and a modulus of ≈10^8 Pa was obtained at 80 °C for the polymer nanocomposite. The nanocomposite solid electrolyte was stable with respect to lithium in a Li|Li symmetrical cell for 1000 h. In addition, in a full solid-state battery using $LiFePO_4$ as the cathode and lithium metal as the anode, a specific capacity of 150 $mAhg^{-1}$ with a current density of 0.05 mA cm^{-2} was achieved.

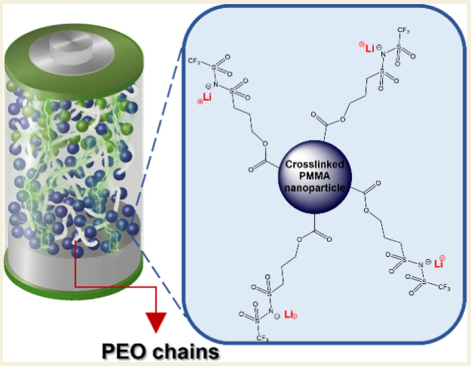

KEYWORDS: *lithium battery, solid polymer electrolyte, nanocomposite polymer electrolyte, Li-polymer nanoparticles, PEO blends*

1. INTRODUCTION

Solid-state lithium−metal batteries are energy storage devices widely studied for application in modern electronics due to the high specific capacity of lithium metal as the anode (3860 $mAhg^{-1}$).[1,2] Nowadays, solid polymer electrolytes based on poly(ethylene oxide) (PEO) are the most successful in commercial solid-state batteries.[3] However, PEO has several limitations. The first one is related to its electrochemical stability window and low lithium transference number (t_{Li}^+ ≈ 0.2), which affect battery operation.[4] To circumvent this limitation, the so-called lithium single-ion conducting polymers have been developed, showing t_{Li}^+ values close to 1. Another limitation is related to its poor mechanical properties at temperatures above its melting temperature. One of the ways to improve the mechanical properties of PEO-based SPEs is by adding inorganic nanoparticles (NPs) or nanowires (e.g., Al_2O_3, MgO, TiO_2, SiO_2),[5] leading to nanocomposite polymer electrolytes. However, inorganic nanoparticles suffer from agglomeration, and low homogeneity of the nanocomposite at high contents of nanoparticles[6] negatively affects the ionic conductivity and the mechanical properties. For improving this, the surface of the inorganic nanoparticle needs to be modified, which is a tedious and not easy step in most cases.

For this reason, the preparation of nanocomposite polymer electrolytes with a lithium single-ion behavior is quite challenging. For example, Villaluenga et al. synthesized salty nanoparticles comprising silsesquioxane cores with covalently bound polystyrenesulfonil lithium (trifluoromethylsulfonyl) imide (PSLiTFSI) by nitroxide-mediated polymerization.[7] In another example, Lago et al. functionalized SiO_2 and Al_2O_3 nanoparticles with lithium [(4-methylphenyl)sulfonyl]-[(trifluoromethyl)sulfonyl] amide, which entails many steps of synthesis and purification.[5] On the other hand, Lechartier et al. developed hybrid solid electrolytes formed by a poly(ethylene glycol) type single-ion polymer network and commercial ceramic nanoparticles of $Li_{7-3X}Al_XLa_3Zr_2O_{12}$ (LLZO); it was observed that the ionic conductivity decreased as the concentration of the nanoparticles increased to more than 40% because the nanoparticles began to agglomerate and settle.[8] Recently, Bocharova et al. prepared single Li-ion

Received: October 12, 2023
Revised: December 4, 2023
Accepted: December 4, 2023
Published: January 16, 2024

conducting hairy nanoparticles of SiO_2 and poly(lithium 1-(3-(methacryloyloxy)propylsulfonyl)-1-(trifluoromethylsulfonyl)-imide) (PLiMTFSI), improving the mechanical properties and the cycling stability of the PEO nanocomposites. However, in all the cases, a lithium salt such as LiTFSI was added to the solid electrolyte in order to study symmetric and full battery cells.[9]

Previously, some of us[6] reported the synthesis of polymeric nanoparticles (100 nm) based on cross-linked poly(methyl methacrylate) (PMMA) functionalized with an lithium sulfonamide methacrylate comonomer. This method allows preparation of acrylic LiNPs, which were easily functionalized having anionic sulfonamide groups with free-mobile lithium cations. All-polymer nanocomposites can be prepared by simply mixing these LiNPs with PEO. However, the ionic conductivity of the first all-polymer nanocomposite was too low for battery applications; therefore, a lithium salt (LiTFSI) was added to the system to reach a functional ionic conductivity for battery operation. However, in this latter case, both $TFSI^-$ and Li^+ ions likely contribute to the conductivity and the lithium-ion transference number (t_{Li^+}) significantly decreases.

In the present work, polymeric nanoparticles of very small size (25 nm) functionalized with lithium sulfonamide groups were synthesized in order to prepare all-polymer nanocomposites by mixing with PEO. The final goal was to develop all-polymer nanocomposite solid electrolytes, which do not require the presence of an additional lithium salt. The preparation of the nanocomposites and the distribution of the NPs within the PEO matrix were first investigated. Then, a deep understanding of how the NPs affected the crystallization of PEO was obtained. The ionic conductivity of the nanocomposite polymer electrolyte was evaluated as a function of its composition as well as the lithium-ion transference number. The salt-free nanocomposite electrolyte with the best ratio between ionic conductivity and mechanical properties was evaluated in a lithium−metal battery as a salt-free solid electrolyte using a $LiFePO_4$ (LFP) as the cathode material.

2. MATERIALS AND METHODS

Poly(ethylene oxide) (100 000 g mol^{-1}, Sigma-Aldrich), methyl methacrylate (MMA, Sigma-Aldrich), ethylene glycol dimethacrylate (EGDMA, Sigma-Aldrich), and lithium 1-(3-(methacryloyloxy)-propylsulfonyl)-1-(trifluoromethylsulfonyl)imide (LiMTFSI) were purchased from Specific Polymers. Lithium dodecyl sulfonate (LiDS, Sigma-Aldrich), ascorbic acid, *tert*-butyl hydroperoxide (70% solution in water, TBHP), acetonitrile (ACN, Sigma-Aldrich), and carbon-coated lithium iron phosphate ($LiFePO_4$) were purchased from Aleees. Carbon black (C65) was purchased from Timcal.

2.1. Synthesis of Lithium Sulfonamide Functional Cross-Linked PMMA Nanoparticles

Lithium-functionalized polymer nanoparticles were synthesized by emulsion polymerization of lithium monomer (LiMTFSI) and methyl methacrylate (MMA), as reported in previous work.[6] This one-pot synthesis was carried out in water at 70 °C with 10% solid content for 6 h, employing ascorbic acid and hydrogen peroxide as a redox initiator system, EGDMA as a cross-linker for PMMA, and LiDS as a surfactant.

In a 100 mL flask, 35 g of Milli-Q water and 0.25 g of LiDS were purged with N_2 for 20 min at 50 °C. Separately, in three different vials, 2.5 g of LiMTFSI (50 wt % respectively total monomer) and 0.114 g of ascorbic acid in 5 g of Milli-Q water; 2.5 g of MMA (50 wt % respectively total monomer) and 0.1 g of EGDMA; and 0.065 mL of H_2O_2 in 5 g of Milli-Q water were predissolved and purged with N_2. After being purged, the three separated solutions were slowly incorporated into the 100 mL flask, and the temperature was increased to 70 °C. The reaction time was set at 6 h.

Coagulated nanoparticles were removed using an 80 mm filter (less than 1 wt %). Finally, LiNPs were purified with Milli-Q water for 5 days at 25 °C employing dialysis tubes with a molecular weight cutoff of 14 000 Da and finally freeze-dried with a Telstar LyoQest-85 Lyophilizer at −80 °C and 0.089 mbar for 3 days.

Lithium-functionalized cross-linked nanoparticles presented an 81% conversion by weight. The NPs' size was determined by DLS, and the results obtained indicated that they had an average diameter of 25 nm (and a 0.298 PDI).

2.2. All-Polymer Nanocomposite Preparation

The all-polymer nanocomposites were prepared by a solvent casting method; PEO was completely dissolved in acetonitrile (ACN), after which the polymer nanoparticles were added, and the solutions were ultrasonicated for 30 min. The solvent was evaporated at room temperature for 24 h; then, the samples were placed in a vacuum oven at 70 °C to remove all remaining solvent.

2.3. Experimental Techniques

Ultrathin sections were cut at −90 °C with a diamond knife on a Leica EMFC6 cryo-ultramicrotome device. The 80 nm thick ultrathin sections were mounted on 300 mesh grids. RuO_4 staining was performed by exposing the thin films to RuO_4 vapor in a 150 mL closed vessel at 20 °C. The staining exposure time was 20 min. A TECNAI G2 20 TWIN transmission electron microscope (TEM) was employed, operating at 200 kV and equipped with a LaB6 filament.

DSC experiments were performed in a PerkinElmer 8000 apparatus fitted with an Intracooler II, and an ultrapure nitrogen atmosphere was used. For nonisothermal experiments, the samples (∼5 mg) were encapsulated in aluminum pans and heated from 25 to 100 °C to erase the thermal history, then cooled to −60 °C, and finally heated to 100 °C; the rate for these experiments was 20 °C min^{-1}. The second heating is presented in the results.

The crystallinity degree was calculated using the following equation

$$X_c = \frac{\Delta H_m}{f \Delta H_m^0} \times 100 \quad (1)$$

where ΔH_m is the melting enthalpy measured during the second heating in the DSC, f is the fraction of PEO in the sample, and ΔH_m^0 is the equilibrium melting enthalpy for PEO; this value is 214 J g^{-1}.[10]

The Gordon−Taylor equation was employed to fit the T_g values with respect to the composition

$$T_{g,blend} = \frac{w_1 T_{g1} + k w_2 T_{g2}}{w_1 + k w_2} \quad (2)$$

where w_1 and w_2 are the polymer component weight fractions, T_{g1} and T_{g2} are the glass transition temperatures of PEO and NPs, respectively, and k is the $\rho_1 \Delta\alpha_2 / \rho_2 \Delta\alpha_1$ ratio. ρ and $\Delta\alpha$ correspond to the density and the expansion coefficient change at T_g, respectively.

For the isothermal crystallization experiments, the T_c range for each sample was determined by the methodology recommended by Müller et al.[11,12] Once the T_c values were chosen, the samples were evaluated as follows: (1) heating from 25 to °C at 20 °C min^{-1}; (2) holding 3 min at 100 °C; (3) cooling to T_c at 60 °C min^{-1}; (4) holding at T_c during 10−40 min to allow crystallization to saturate; and (5) heating from T_c to 100 °C at 20 °C min^{-1} to register the melting temperature after isothermal crystallization.

The mechanical properties of the selected electrolyte were measured by dynamic mechanic thermal analysis (DMTA) in tension mode with a Triton 2000 DMA (Triton Technology). The experiments were carried out at 1 Hz, with a heating rate of 4 °C min^{-1}, from −100 to 80 °C, using rectangular samples of 1 × 1 × 0.1 cm^3.

The ionic conductivity was calculated by electrochemical impedance spectroscopy (EIS) using an Autolab 302N potentiostat galvanostat equipped with a Microcell HC station for temperature control at different temperatures in the range of 90−40 °C. The

https://doi.org/10.1021/acspolymersau.3c00035
ACS Polym. Au 2024, 4, 77−85

sample was placed in the cell between two 10 mm diameter stainless-steel electrodes. The experiments were performed in the 100 kHz−1 Hz range, with 10 mV of amplitude. All of the samples had an average thickness of 0.1 mm.

For Li−Li symmetrical cell experiments, membranes of PEO 50 wt % LiNP electrolyte were obtained by compression molding at 120 °C (∼120 μm thick). Li ribbons (100 μm) were cleaned with cyclohexane with a nylon brush in an Ar glovebox. Subsequently, 0.5 cm^2 disks of Li were punched to assemble the different cells, which were all characterized at 80 °C. The cathodic stability was tested in Li|Li symmetrical cells in the range from −0.5 to 2 V, which were fabricated by sandwiching the polymeric membranes between two lithium disks in the CR2032 coin cell setup. Anodic stability was evaluated in Li|SS cells in the range from 3 to 7 V vs Li^0/Li^+. Fresh Li|Li symmetrical cells were also employed to characterize lithium transference number, long-term plating−stripping, and ramp tests. For lithium-ion transference number (t_{Li}^+) measurement, EIS was used in the range of 1 MHz−1 Hz with a perturbation of 40 mV and a polarization potential of 80 mV for 4 h after 10 h of resting. The Bruce−Vincent−Evans method was applied to determine t_{Li}^+ according to the following equation[13]

$$t_{Li}^+ = \frac{I_s(\Delta V - I_0R_0)}{I_0(\Delta V - I_sR_s)} \quad (3)$$

where ΔV is the applied potential across the cell, I is the current, R is the interfacial resistance, and the subscripts s and 0 are the steady-state and initial values, respectively.

Plating−stripping was also evaluated in long-term experiments at 0.1 mA cm^{-2} for 1000 h (1 h of plating and 1 h of stripping). DC polarization was investigated by measuring the initial impedance and performing a subsequent ramp test in the range 0.02−0.50 mA cm^{-2}. In this experiment, the voltage value is measured as a function of current density, and the resistance value is constant, so by applying Ohm's law we can obtain the theoretical voltage values for the measured current densities. The information provided by this experiment is to know the range of current densities within which the electrolyte conforms to Ohm's law (indicating that it behaves as a single-ion polymer electrolyte).

LFP positive electrodes were fabricated by using a slurry containing 60 wt % of LFP, 30 wt % of catholyte (PEO 50 wt % LiNPs), and 10 wt % of C65. The resultant formulation was coated on aluminum foil and left to dry at room temperature for 12 h. Afterward, the obtained cathode was further dried at 60 °C under vacuum for 12 h and then punched (0.5 cm^{-2}). The average mass loading of the electrodes was 1.3 mg_{LFP} cm^{-2}. The Li|PEO-NPs|LFP full cell was assembled by sandwiching a PEO-NPs film between a lithium metal anode (12 mm in diameter) and LFP cathode (8 mm in diameter). Subsequently, the cell was cycled galvanostatically in the 3.8−2.8 V vs Li^0/Li^+ range at C/10 (0.05 mA cm^{-2}), considering the theoretical specific capacity of LFP (170 $mAhg^{-1}$).

A VMP-3 potentiostat and Neware battery cycler were employed for electrochemical measurements.

3. RESULTS AND DISCUSSION

3.1. Preparation of All-Polymer Nanocomposites

Figure 1a shows the chemical structure of the repeating unit of the synthesized LiNPs that were based on a cross-linked copolymer between MMA and LiMTFSI monomers. Cross-linked PMMA nanoparticles with lithium sulfonamide groups were obtained by emulsion polymerization as reported before. By tuning the copolymer composition and the use of surfactant, very small NPs were synthesized. Figure 1b shows a TEM image of the polymer nanoparticles, which show a size between 25 and 30 nm. The all-polymer nanocomposites investigated in this article were prepared by solvent casting from acetonitrile with different weight ratios between PEO and

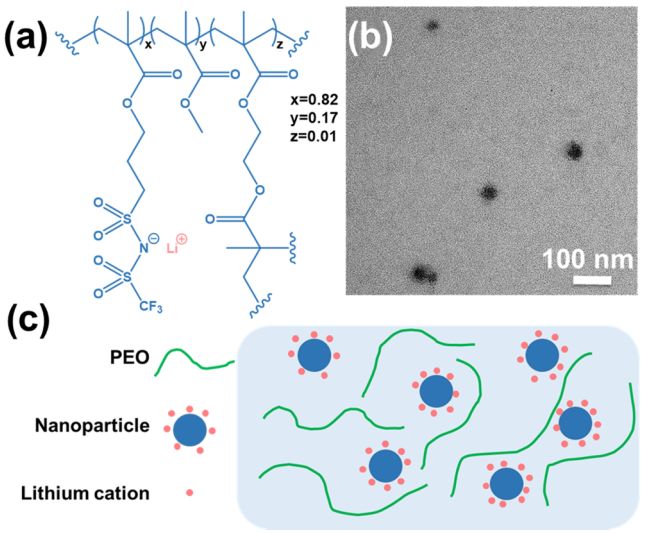

Figure 1. (a) Chemical structure of the synthesized copolymer, (b) TEM image of the nanoparticles cross-linked poly(MMA-*co*-LiMTFSI), and (c) schematic representation of the all-polymer nanocomposites.

the LiNP; Figure 1c is a schematic representation of the composites PEO/LiNPs.

3.2. Characterization of All-Polymer Nanocomposites by Transmission Electron Microscopy (TEM)

In order to visualize the dispersion of the LiNPs within the PEO matrix, TEM was carried out. Figure 2 shows the TEM images for the four compositions with a staining agent (ruthenium tetroxide); the size of the nanoparticles is between 20 and 30 nm as mentioned above, and the background is the PEO matrix. A greater number of particles per unit area is observed as the concentration of nanoparticles in PEO increases. Interestingly the LiNPs are very well dispersed in the PEO matrix without signs of agglomeration for PEO 15 wt % LiNPs and PEO 30 wt % LiNPs between LiNPs and PEO (Figure 2a,b).

In the PEO 50 wt % LiNPs, a higher amount of LiNPs with a good dispersion is observed; however, there are some particles that are together in pairs (Figure 2c). For the PEO 70 wt % LiNPs, due to the large amount of LiNPs, it was not possible to clearly observe the distribution of the LiNPs (Figure S1); for this reason, the fluor-energy-dispersive X-ray spectroscopy (F-EDS) technique was used, since it is a technique that helps us to find chemical elements in the sample using the interaction that exists between the sample and the electron beam.[14] In Figure 2d, the blue dots correspond to where there are fluorine atoms and the black background is the PEO; this gives us an idea of the distribution of the LiNPs in the PEO, and with this concentration of NPs, there are certain regions where there are agglomerations of NPs. One of the main advantages of using polymeric NPs is that the dispersion in the PEO matrix is much more homogeneous, even at high concentrations.

3.3. PEO Crystallization Studies in All-Polymer Nanocomposites

3.3.1. Nonisothermal DSC Results. Figure 3a shows the second DSC heating scans for neat PEO and the different blends varying the concentration of LiNPs between 15 and 70 wt % (solid lines) and also the second heating for PEO/PMMA NPs blends without the incorporation of the single-ion

https://doi.org/10.1021/acspolymersau.3c00035
ACS Polym. Au 2024, 4, 77−85

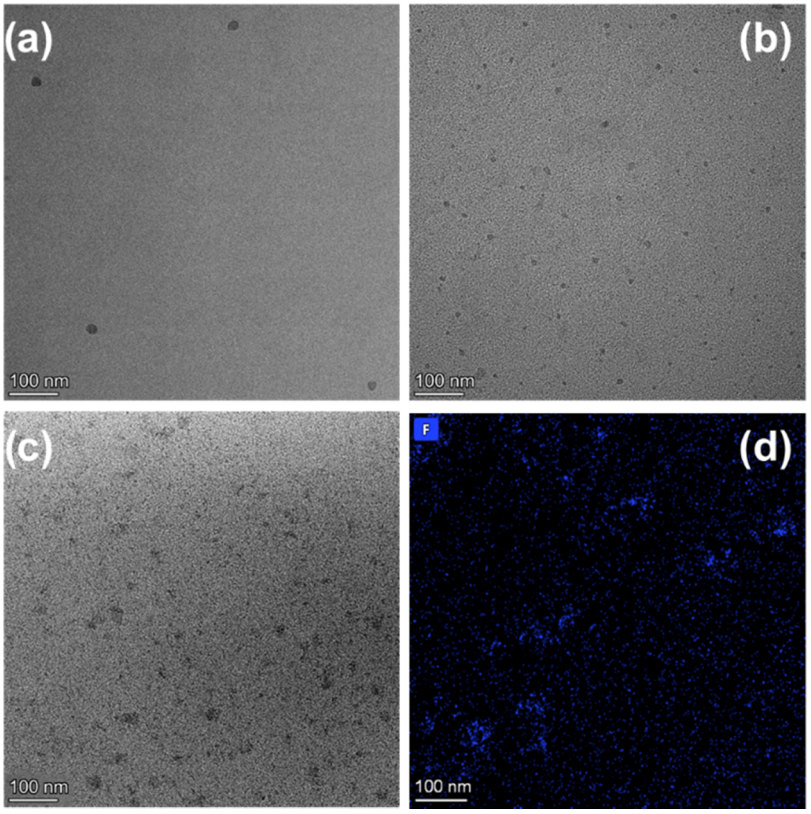

Figure 2. TEM images for the polymer nanocomposites (a) PEO 15 wt % LiNPs, (b) PEO 30 wt % LiNPs, (c) PEO 50 wt % LiNPs, and (d) PEO 70 wt % LiNPs.

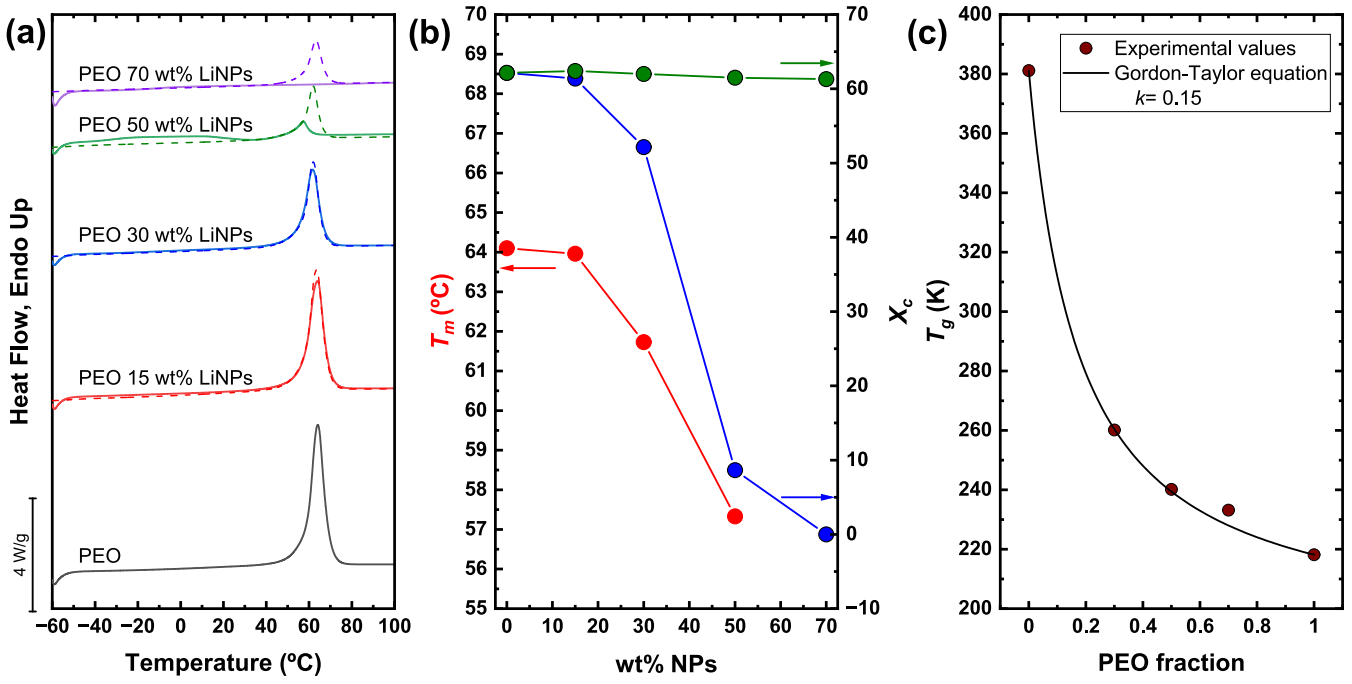

Figure 3. (a) DSC second heating for neat PEO and different polymer nanocomposites (PEO/LiNPs, solid lines and PEO/PMMA NPs, dashed lines), (b) melting temperature (T_m) for the blends PEO/LiNPs and crystallinity degree (X_c) of the blends as a function of wt % NPs (blue dots for the blends PEO/LiNPs and green dots for the blends PEO/PMMA NPs), and (c) T_g of the blends as a function of PEO fraction.

monomer (dashed lines). The latter samples were prepared as a reference to see the effect of the single-ion monomer presence in the nanoparticle on the crystallization of the PEO. For the PEO/LiNPs system, the melting temperature of PEO decreases from 64 to 57 °C with 50 wt % LiNPs, and with 70 wt % LiNPs, the PEO becomes amorphous. In the case of the PEO/PMMA NPs system, the T_m of PEO remains constant, indicating that, although PMMA and PEO are miscible

https://doi.org/10.1021/acspolymersau.3c00035
ACS Polym. Au 2024, 4, 77−85

polymers,[15−17] once the PMMA is cross-linked, their miscibility disappears, as cross-linked PMMA does not allow the penetration of PEO chains within the NPs. Table S1 shows the melting temperatures and enthalpy values of the PEO/LiNPs blends.

Figure 3b shows the change in the PEO melting temperature (T_m) and degree of crystallization (X_c) for both systems. As the NPs containing cross-linked PMMA are not miscible (green dots) with PEO, the PEO degree of crystallinity remains constant and independent of NP concentration. However, the presence of LiMTFSI on the surface of the LiNPs results in an interaction of the ionic groups with PEO. Such interactions affect both T_m (red dots) and X_c (blue dots). A similar effect has been reported before for the PEO/PLiMTFSI linear polymer blend system where these interactions restrict the crystallization of PEO.[18]

The interactions between LiNPs and PEO are also reflected in the change in the T_g of the blends; the T_g increases with the increasing concentration of NPs in the blend and only presents an intermediate value between the T_g of PEO and the T_g of LiNPs (Figure 3c), indicating that the T_g of the blend depends on the composition. Furthermore, the experimental values obtained fit to the Gordon−Taylor eq (eq 2).[19,20]

3.3.2. Overall Crystallization Rate. One of the ways to study the effect of LiNPs on PEO crystallization is by quantitatively determining the overall crystallization kinetics by DSC isothermal experiments. Isothermal crystallization in the DSC encompasses crystal nucleation and crystal growth, and the inverse of the half relative crystallization time ($1/\tau_{50\%}$) is an experimental measure of crystallization rate. Figure 4 shows the overall crystallization rate for neat PEO and for the PEO component in the 95/5, 85/15, and 70/30 blends in which PEO can crystallize. It is observed that the crystallization rate and the supercooling needed for the PEO component to crystallize decrease with the increasing concentration of nanoparticles in the system. Once again, the results can be explained by the interactions between the PLiMTFSI and PEO chains, which reduce the availability of PEO chains in the crystallization front.

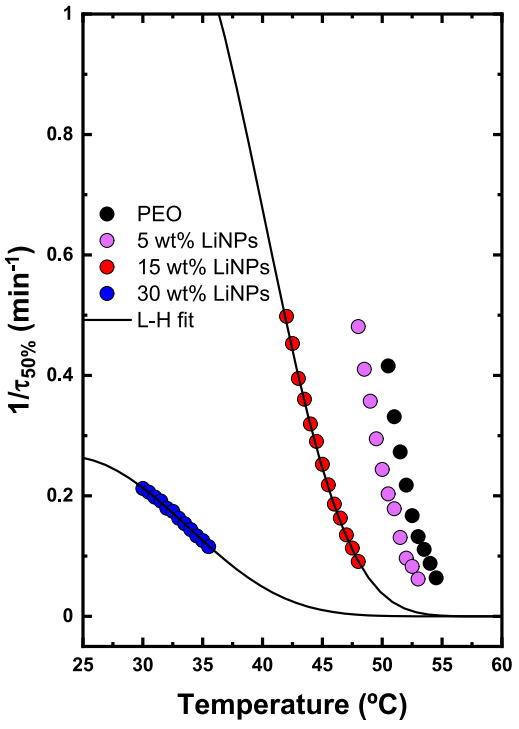

Figure 4. Overall crystallization rate as a function of temperature for neat PEO and the polymer nanocomposites 95/5, 85/15, and 70/30.

3.4. Ionic Conductivity, Lithium-Ion Transference Number (t_{Li}^+), and Mechanical Properties

Ionic conductivity is one of the more critical parameters to consider for applying a solid electrolyte in an electrochemical application such as in a battery. Figure 5a shows the ionic conductivity calculated by electrochemical impedance spectroscopy (EIS) as a function of the temperature for the different polymer nanocomposites. The ionic conductivity increases as a function of temperature, as expected for an activated process. However, a very pronounced drop in ionic conductivity is observed in the 85/15 and 70/30 electrolytes around 60 °C due to crystallization of PEO (Figure 3a). The highest ionic conductivity values at 80 °C were obtained with the PEO 30 wt % LiNPs and PEO 50 wt % LiNPs samples, being 1.1×10^{-5} and 8.4×10^{-6} S cm^{-1}, respectively. In the case of the PEO 50 wt % LiNPs blend, it presents a small change in slope around 50 °C; this change is smaller compared to the previous mixtures because the crystallinity of this electrolyte is much lower. In the PEO 70 wt % LiNPs, the ionic conductivity is in the order of 10^{-7} S cm^{-1} at 90 °C; although it is the electrolyte with the highest amount of LiNPs, the ionic conductivity values are the lowest, due to the fact that this material is very rigid (higher T_g).[21] In addition, as seen in the TEM images in this composition, there is some agglomeration of the LiNPs, which is also reflected in the ionic conductivity. These results indicate that ion mobility is the parameter that makes the greatest contribution to ionic conductivity over the amount of ions present in the electrolyte.[18,22]

The PEO 50 wt % LiNPs composite electrolyte was selected for further electrochemical studies since it showed the best relationship between ionic conductivity and qualitative mechanical properties. The t_{Li}^+ value is related to the fraction of the ionic conductivity due to the movement of the lithium cations and is typically low for polymers with dissolved salt due to the predominance of the anion diffusion; for the PEO/LiTFSI system, the t_{Li}^+ is about 0.2.[23] Using the Bruce−Vincent−Evans method (eq 3), the lithium-ion transference number (t_{Li}^+) was calculated for the blend PEO 50 wt % LiNPs at 80 °C (Figure 5b and Table S2). A value of 0.68 was obtained, which is not as high as expected for a lithium single-ion conductor (typically > 0.85). However, in other articles, similar values have been reported and this was associated with the movement of sulfonamide groups attached to the polymer backbone. In principle, this value of the lithium transport number higher than those of the conventional PEO solid electrolytes should have beneficial effect on the safety of the battery, since it affects the growth of lithium dendrites.[24,25]

The DMTA measurement was performed for this electrolyte to quantify the mechanical properties as one of the advantages of using NPs in the electrolyte is to improve the mechanical properties.[26,27] Figure 6 presents the storage modulus as a function of temperature for the PEO 50 wt % LiNPs electrolyte and compares it with the neat PEO reference. At low temperatures, a modulus on the order of ~10^9 Pa is observed for both samples, which corresponds to the glassy state. The main difference is observed in the T_g of the materials; in the case of neat PEO, the T_g is −51 °C, and for the blend PEO 50

https://doi.org/10.1021/acspolymersau.3c00035
ACS Polym. Au 2024, 4, 77−85

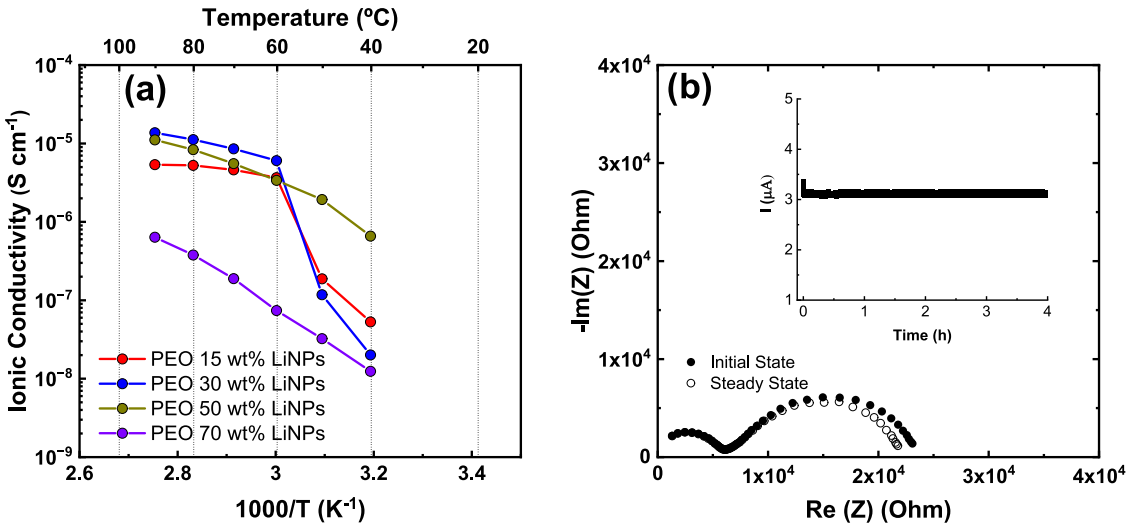

Figure 5. (a) Ionic conductivity as a function of temperature for the different polymer nanocomposites and (b) ac- and dc-measurements for the lithium-ion transference number measurements for PEO 50 wt % LiNPs electrolyte.

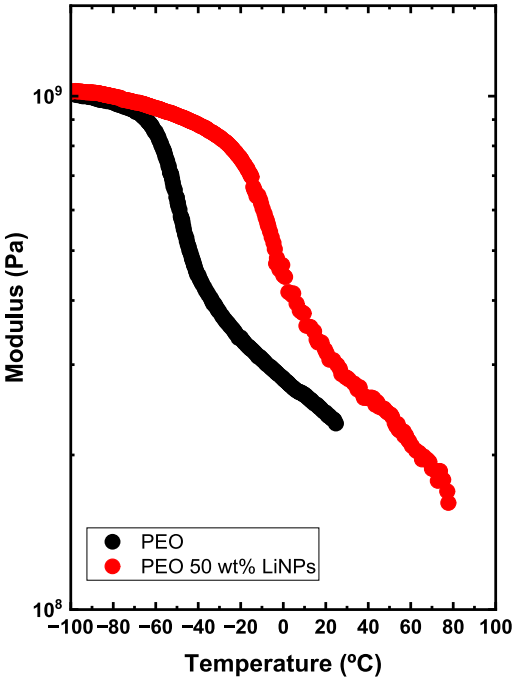

Figure 6. DMTA of neat PEO and the polymer nanocomposite PEO 50 wt % LiNPs as a function of temperature.

wt % LiNPs, the T_g is around 0 °C. The subsequent melting of the PEO makes it impossible to measure the elastic modulus at higher temperatures. However, in the blend PEO 50 wt % LiNPs, it is possible to obtain a modulus value even at higher temperatures. This confirms that the polymer nanocomposites show a mechanical reinforcement of the PEO by the incorporation of the polymer nanoparticles.

3.5. Electrochemical Characterization

Another way to prove that the electrolyte behaves as a single-ion polymer electrolyte is to obtain the overpotential value at different current densities in a symmetrical Li cell. Equation 4 reported by Mehrotra et al.[28] was used to describe the behavior of the electrolyte

$$\nabla\Phi = -\frac{i}{k} + \frac{2RT}{F}(1 - t^{+})\left(1 + \frac{d\ln f}{d\ln c}\right)\frac{\nabla c}{c} \tag{4}$$

where ϕ is the potential, k is the ionic conductivity of the electrolyte, F is Faraday's constant, $1 + \frac{d\ln f}{f\ln c}$ is the thermodynamic factor, t^{+} is the transference number, and c is the concentration. The first term of this equation represents the Ohmic drop, and the second term represents the concentration overpotential in the electrolyte. For single-ion electrolytes, the potential would be given purely by the Ohmic drop since there are no more species to polarize. Figure 7 shows the potential as a function of different current densities applied to a symmetrical cell (as taken from Figures S2 and S3). The line represents Ohm's equation, and the blue dots are the obtained experimental data. If the data conform to Ohm's equation, this

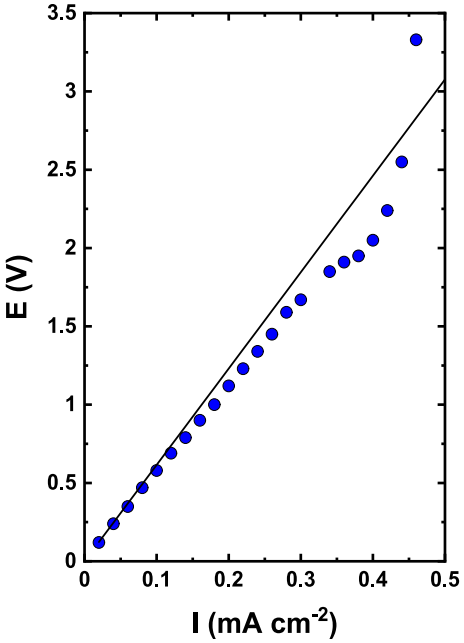

Figure 7. Experimental $I-V$ curves for a Li−Li symmetrical cell. The solid line is the Ohm equation.

https://doi.org/10.1021/acspolymersau.3c00035
ACS Polym. Au 2024, 4, 77−85

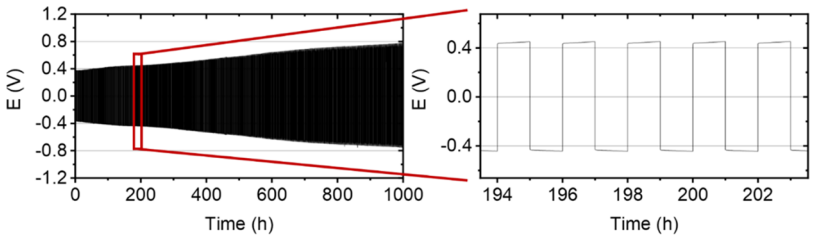

Figure 8. Potential as a function of time for symmetrical lithium cells for the polymer nanocomposite electrolyte PEO 50 wt % LiNPs cycled at 0.05 mA cm^{-2} at 80 °C.

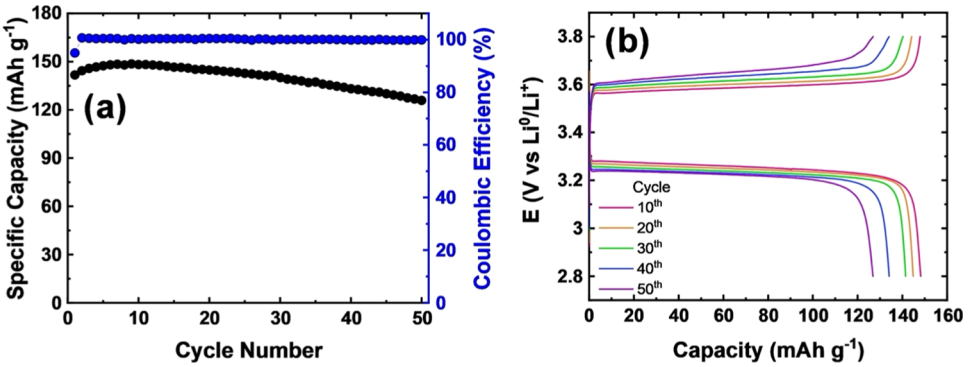

Figure 9. (a) Specific capacity and Coulombic efficiency as a function of cycle number and (b) voltage profiles at different cycles.

indicates that the electrolyte behaves as a single-ion polymer electrolyte, as was observed at low current densities. However, as the applied current density increases, the experimental value moves away from ideality. These results indicate that the system behaves as a single-ion electrolyte up to 0.13 mA cm^{-2}. This is consistent with the value of the transport number; possibly at higher current densities, the nanoparticles have larger mobilities, which drive the values away from ideality.

Figure 8 presents the Li metal plating and stripping measurements at 80 °C for the PEO 50 wt % LiNPs electrolyte since it presents a good relationship between ionic conductivity and mechanical properties. The cell was cycled for 1000 h at 0.05 mA cm^{-2} because, as shown in Figure 7, the electrolyte behaves as a single-ion polymer electrolyte at this current density, showing high reversibility of the lithium plating/stripping cycles in this electrolyte. The overpotential increased from 0.4 to 0.8 V after 1000 h. The stability with cycling indicates that the electrolyte avoids critical dendrite formation.[29]

Figure S4 presents the cationic and anionic stability of the electrolyte PEO 50 wt % LiNPs at 80 °C. During the cathodic scan (Figure S4a), reversible oxidation and reduction peaks corresponding to the plating and stripping of lithium are observed, respectively. The anodic stability of the proposed electrolyte is limited by the nature of the host polymer,[30] which typically shows a minor oxidation (~10 μA cm^{-2}) around 4 V.[31,32] To further study the electrolyte potential, lithium iron phosphate (LFP) was selected as the cathode active material due to its compatibility with PEO.

The electrochemical performance of the electrolyte PEO 50 wt % LiNPs was evaluated in a battery cell consisting of a lithium metal anode and $LiFePO_4$ (LFP) cathode (60 wt % active material/30 wt % solid electrolyte/10 wt % C65). The cell was assembled by sandwiching a PEO 50 wt % LiNPs membrane between the two electrodes. Unfortunately, we could not have a comparison with a PEO/LiTFSI electrolyte probably due to the softness of this solid electrolyte at 80 °C. Figure 9a shows the specific capacity and Coulombic efficiency as functions of the cycle number. The cell was tested at C/10 between 3.8 and 2.8 V. The Coulombic efficiency is 100% during the 50 cycles; in addition, a specific capacity of 150 $mAhg^{-1}$ was obtained, representing 88% with respect to the theoretical capacity of $LiFePO_4$; this value decreases to 125 $mAhg^{-1}$ in the 50th cycle.

Figure 9b presents the voltage profiles during the different cycles. We observe that the specific capacitance decreases as the number of cycles increases, and also the voltage difference between charge and discharge increases during the cycles; this same effect is observed in the plating/stripping in Figure 8, indicating the possible formation of a more resistive SEI, which adds to the cell resistance.

4. CONCLUSIONS

In this paper, a salt-free all-polymer nanocomposite solid electrolyte for lithium metal batteries is presented. This all-polymer nanocomposite was prepared by casting blends of PEO with lithium sulfonamide-functionalized poly(methyl methacrylate) nanoparticles (LiNPs) of very small size (25 nm). It was found that LiNPs are well dispersed in PEO, with a small degree of agglomeration evident only at very high concentrations of LiNPs (50 and 70 wt %). Using DSC, it was shown that by increasing the concentration of nanoparticles in the system, the crystallinity of PEO decreases and that the interactions of PLiMTFSI in the nanoparticle with PEO are the causes of the decrease in the crystallinity of PEO. The ionic conductivity at temperatures above the melting temperature of PEO is of the order of 10^{-5} S cm^{-1}; as the concentration of LiNPs increases to more than 70 wt %, the ionic conductivity decreases due to the rigidity of the system and the agglomeration of the LiNPs. The 50:50 wt % LiNP/PEO nanocomposite showed the best compromise between ionic conductivity, high lithium transference number, and mechan-

https://doi.org/10.1021/acspolymersau.3c00035
ACS Polym. Au 2024, 4, 77−85

ical properties. Furthermore, it was shown that the storage modulus of the electrolyte increases with the incorporation of LiNPs with respect to neat PEO while maintaining a high value at temperatures higher than PEO T_m.

Finally, the all-polymer nanocomposite (PEO 50 wt % LiNPs) was studied as a solid electrolyte in lithium metal batteries. The all-polymer nanocomposite behaved as a single-ion polymer electrolyte up to a current density of 0.13 mA cm. In a symmetrical Li/Li cell, the electrolyte was stable with respect to lithium for more than 1000 h. Moreover, a full lithium−metal cell (Li|PEO 50 wt % LiNPs|LFP) was successfully cycled obtaining 150 $mAhg^{-1}$ without the need of free lithium salt added into the electrolyte.

■ ASSOCIATED CONTENT

Supporting Information

The Supporting Information is available free of charge at https://pubs.acs.org/doi/10.1021/acspolymersau.3c00035.

TEM and F-EDS of sample PEO 70 wt % LiNPs; data of nonisothermal DSC (T_m, ΔH_m, and T_g); values used to calculate the lithium-ion transference number; and change in voltage as a function of different current densities for the electrolyte PEO 50 wt % LiNPs (PDF)

■ AUTHOR INFORMATION

Corresponding Authors

Alejandro J. Müller − *POLYMAT and Department of Polymers and Advanced Materials: Physics, Chemistry and Technology, Faculty of Chemistry, University of the Basque Country UPV/EHU, 20018 Donostia-San Sebastián, Spain; IKERBASQUE, Basque Foundation for Science, 48009 Bilbao, Spain;* orcid.org/0000-0001-7009-7715; Email: alejandrojesus.muller@ehu.es

David Mecerreyes − *POLYMAT and Department of Polymers and Advanced Materials: Physics, Chemistry and Technology, Faculty of Chemistry, University of the Basque Country UPV/EHU, 20018 Donostia-San Sebastián, Spain; IKERBASQUE, Basque Foundation for Science, 48009 Bilbao, Spain;* orcid.org/0000-0002-0788-7156; Email: david.mecerreyes@ehu.es

Authors

Jorge L. Olmedo-Martínez − *POLYMAT and Department of Polymers and Advanced Materials: Physics, Chemistry and Technology, Faculty of Chemistry, University of the Basque Country UPV/EHU, 20018 Donostia-San Sebastián, Spain*

Rafael Del Olmo − *POLYMAT and Department of Polymers and Advanced Materials: Physics, Chemistry and Technology, Faculty of Chemistry, University of the Basque Country UPV/EHU, 20018 Donostia-San Sebastián, Spain;* orcid.org/0000-0002-0906-0523

Antonela Gallastegui − *POLYMAT and Department of Polymers and Advanced Materials: Physics, Chemistry and Technology, Faculty of Chemistry, University of the Basque Country UPV/EHU, 20018 Donostia-San Sebastián, Spain*

Irune Villaluenga − *POLYMAT and Department of Polymers and Advanced Materials: Physics, Chemistry and Technology, Faculty of Chemistry, University of the Basque Country UPV/EHU, 20018 Donostia-San Sebastián, Spain; IKERBASQUE, Basque Foundation for Science, 48009 Bilbao, Spain*

Maria Forsyth − *POLYMAT and Department of Polymers and Advanced Materials: Physics, Chemistry and Technology, Faculty of Chemistry, University of the Basque Country UPV/EHU, 20018 Donostia-San Sebastián, Spain; IKERBASQUE, Basque Foundation for Science, 48009 Bilbao, Spain; Institute for Frontier Materials and Industry Training Transformation Centre for Future Energy Storage Technologies (StorEnergy), Deakin University, Burwood 3125 Victoria, Australia;* orcid.org/0000-0002-4273-8105

Complete contact information is available at: https://pubs.acs.org/10.1021/acspolymersau.3c00035

Author Contributions

J.L.O.M.: Investigation, methodology, data curation, formal analysis, and writing—original draft. R.d.O.: Methodology, data curation, and formal analysis. A.G.: Methodology. I.V.: Validation and resources. M.F.: Conceptualization and validation. A.J.M.: Formal analysis, validation, supervision, resources, and writing—review and editing. D.M.: Visualization, conceptualization, validation, supervision, resources, founding acquisition, and writing—review and editing. CRediT: **Jorge L. Olmedo-Martínez** data curation, formal analysis, investigation, writing-original draft; **Rafael Del Olmo** investigation, methodology, writing-original draft; **Antonela Gallastegui** investigation; **Irune Villaluenga** funding acquisition, writing-review & editing; **Maria Forsyth** conceptualization; **Alejandro J. Müller** resources, supervision, writing-review & editing; **David Mecerreyes** conceptualization, resources, writing-review & editing.

Notes

The authors declare no competing financial interest.

■ ACKNOWLEDGMENTS

Financial support of the Spanish Agencia Estatal de Investigación of the MINECO through project PID2020-119026GB-I00 and the Basque Government, Department of Educatiom through PIBA_2021_1_0025 is acknowledged.

■ REFERENCES

(1) He, F.; Tang, W.; Zhang, X.; Deng, L.; Luo, J. High Energy Density Solid State Lithium Metal Batteries Enabled by Sub-5 Mm Solid Polymer Electrolytes. *Adv. Mater.* **2021**, *33* (45), No. 2105329.

(2) Zhang, H.; Li, C.; Piszcz, M.; Coya, E.; Rojo, T.; Rodriguez-Martinez, L. M.; Armand, M.; Zhou, Z. Single Lithium-Ion Conducting Solid Polymer Electrolytes: Advances and Perspectives. *Chem. Soc. Rev.* **2017**, *46* (3), 797−815.

(3) Nair, J. R.; Imholt, L.; Brunklaus, G.; Winter, M. Lithium Metal Polymer Electrolyte Batteries: Opportunities and Challenges. *Electrochem. Soc. Interface* **2019**, *28* (2), 55.

(4) Piszcz, M.; Garcia-Calvo, O.; Oteo, U.; Lopez del Amo, J. M.; Li, C.; Rodriguez-Martinez, L. M.; Youcef, H. B.; Lago, N.; Thielen, J.; Armand, M. New Single Ion Conducting Blend Based on PEO and PA-LiTFSI. *Electrochim. Acta* **2017**, *255*, 48−54.

(5) Lago, N.; Garcia-Calvo, O.; Lopez del Amo, J. M.; Rojo, T.; Armand, M. All-solid-state Lithium-ion Batteries with Grafted Ceramic Nanoparticles Dispersed in Solid Polymer Electrolytes. *ChemSusChem* **2015**, *8* (18), 3039−3043.

(6) Porcarelli, L.; Sutton, P.; Bocharova, V.; Aguirresarobe, R. H.; Zhu, H.; Goujon, N.; Leiza, J. R.; Sokolov, A.; Forsyth, M.; Mecerreyes, D. Single-Ion Conducting Polymer Nanoparticles as Functional Fillers for Solid Electrolytes in Lithium Metal Batteries. *ACS Appl. Mater. Interfaces* **2021**, *13* (45), 54354−54362.

(7) Villaluenga, I.; Inceoglu, S.; Jiang, X.; Chen, X. C.; Chintapalli, M.; Wang, D. R.; Devaux, D.; Balsara, N. P. Nanostructured Single-Ion-Conducting Hybrid Electrolytes Based on Salty Nanoparticles and Block Copolymers. *Macromolecules* **2017**, *50* (5), 1998−2005.
(8) Lechartier, M.; Porcarelli, L.; Zhu, H.; Forsyth, M.; Guéguen, A.; Castro, L.; Mecerreyes, D. Single-Ion Polymer/LLZO Hybrid Electrolytes with High Lithium Conductivity. *Mater. Adv.* **2022**, *3* (2), 1139−1151.
(9) Bocharova, V.; Chen, X. C.; Jeong, S. P.; Zhou, Z.; Sacci, R. L.; Keum, J. K.; Gainaru, C.; Rahman, M. A.; Sahori, R.; Sun, X.-G.; et al. Single Ion Conducting Hairy Nanoparticle Additive to Improve Cycling Stability of Solid Polymer Electrolytes. *ACS Appl. Energy Mater.* **2023**, *6* (15), 8042−8052.
(10) Beaumont, R. H.; Clegg, B.; Gee, G.; Herbert, J. B. M.; Marks, D. J.; Roberts, R. C.; Sims, D. Heat Capacities of Propylene Oxide and of Some Polymers of Ethylene and Propylene Oxides. *Polymer* **1966**, *7* (8), 401−417.
(11) Lorenzo, A. T.; Arnal, M. L.; Albuerne, J.; Müller, A. J. DSC Isothermal Polymer Crystallization Kinetics Measurements and the Use of the Avrami Equation to Fit the Data: Guidelines to Avoid Common Problems. *Polym. Test.* **2007**, *26* (2), 222−231.
(12) Pérez-Camargo, R. A.; Liu, G. M.; Wang, D. J.; Müller, A. J. Experimental and Data Fitting Guidelines for the Determination of Polymer Crystallization Kinetics. *Chin. J. Polym. Sci.* **2022**, *40*, 658−691.
(13) Evans, J.; Vincent, C. A.; Bruce, P. G. Electrochemical Measurement of Transference Numbers in Polymer Electrolytes. *Polymer* **1987**, *28* (13), 2324−2328.
(14) Son, D.; Cho, S.; Nam, J.; Lee, H.; Kim, M. X-Ray-Based Spectroscopic Techniques for Characterization of Polymer Nanocomposite Materials at a Molecular Level. *Polymers* **2020**, *12* (5), 1053.
(15) Zhang, C.; Liu, X.; Liu, H.; Wang, Y.; Guo, Z.; Liu, C. Multi-Walled Carbon Nanotube in a Miscible PEO/PMMA Blend: Thermal and Rheological Behavior. *Polym. Test.* **2019**, *75*, 367−372.
(16) Lodge, T. P.; Wood, E. R.; Haley, J. C. Two Calorimetric Glass Transitions Do Not Necessarily Indicate Immiscibility: The Case of PEO/PMMA. *J. Polym. Sci., Part B: Polym. Phys.* **2006**, *44* (4), 756−763.
(17) Dionísio, M.; Fernandes, A. C.; Mano, J. F.; Correia, N. T.; Sousa, R. C. Relaxation Studies in PEO/PMMA Blends. *Macromolecules* **2000**, *33* (3), 1002−1011.
(18) Olmedo-Martínez, J. L.; Porcarelli, L.; Alegría, Á.; Mecerreyes, D.; Müller, A. J. High Lithium Conductivity of Miscible Poly(Ethylene Oxide)/Methacrylic Sulfonamide Anionic Polyelectrolyte Polymer Blends. *Macromolecules* **2020**, *53* (11), 4442−4453.
(19) Kalogeras, I. M.; Brostow, W. Glass Transition Temperatures in Binary Polymer Blends. *J. Polym. Sci., Part B: Polym. Phys.* **2009**, *47* (1), 80−95.
(20) Schneider, H. A. The Gordon-Taylor Equation. Additivity and Interaction in Compatible Polymer Blends. *Makromol. Chem.* **1988**, *189* (8), 1941−1955.
(21) Sun, C.; Liu, J.; Gong, Y.; Wilkinson, D. P.; Zhang, J. Recent Advances in All-Solid-State Rechargeable Lithium Batteries. *Nano Energy* **2017**, *33*, 363−386.
(22) Olmedo-Martínez, J. L.; Fdz De Anastro, A.; Martínez-Ibañez, M.; Müller, A. J.; Mecerreyes, D. Polyethylene Oxide/Sodium Sulfonamide Polymethacrylate Blends as Highly Conducting Single-Ion Solid Polymer Electrolytes. *Energy Fuels* **2023**, *37* (7), 5519−5529.
(23) Pożyczka, K.; Marzantowicz, M.; Dygas, J. R.; Krok, F. Ionic Conductivity and Lithium Transference Number of Poly(Ethylene Oxide):LiTFSI System. *Electrochim. Acta* **2017**, *227*, 127−135.
(24) Brissot, C.; Rosso, M.; Chazalviel, J. N.; Lascaud, S. Dendritic Growth Mechanisms in Lithium/Polymer Cells. *J. Power Sources* **1999**, *81-82*, 925−929.
(25) Barai, P.; Higa, K.; Srinivasan, V. Lithium Dendrite Growth Mechanisms in Polymer Electrolytes and Prevention Strategies. *Phys. Chem. Chem. Phys.* **2017**, *19* (31), 20493−20505.
(26) Qin, H.; Fu, K.; Zhang, Y.; Ye, Y.; Song, M.; Kuang, Y.; Jang, S.-H.; Jiang, F.; Cui, L. Flexible Nanocellulose Enhanced Li+ Conducting Membrane for Solid Polymer Electrolyte. *Energy Storage Mater.* **2020**, *28*, 293−299.
(27) Meesorn, W.; Shirole, A.; Vanhecke, D.; de Espinosa, L. M.; Weder, C. A Simple and Versatile Strategy to Improve the Mechanical Properties of Polymer Nanocomposites with Cellulose Nanocrystals. *Macromolecules* **2017**, *50* (6), 2364−2374.
(28) Mehrotra, A.; Ross, P. N.; Srinivasan, V. Quantifying Polarization Losses in an Organic Liquid Electrolyte/Single Ion Conductor Interface. *J. Electrochem. Soc.* **2014**, *161* (10), A1681.
(29) Malunavar, S.; Gallastegui, A.; Wang, X.; Makhlooghiazad, F.; Mecerreyes, D.; Armand, M.; Galceran, M.; Howlett, P. C.; Forsyth, M. Formulation and Characterization of PS-Poly (Ionic Liquid) Triblock Electrolytes for Sodium Batteries. *ACS Appl. Polym. Mater.* **2022**, *4* (12), 8977−8986.
(30) Aldalur, I.; Martinez-Ibañez, M.; Krztoń-Maziopa, A.; Piszcz, M.; Armand, M.; Zhang, H. Flowable Polymer Electrolytes for Lithium Metal Batteries. *J. Power Sources* **2019**, *423*, 218−226.
(31) Aldalur, I.; Martinez-Ibañez, M.; Piszcz, M.; Rodriguez-Martinez, L. M.; Zhang, H.; Armand, M. Lowering the Operational Temperature of All-Solid-State Lithium Polymer Cell with Highly Conductive and Interfacially Robust Solid Polymer Electrolytes. *J. Power Sources* **2018**, *383*, 144−149.
(32) Mindemark, J.; Lacey, M. J.; Bowden, T.; Brandell, D. Beyond PEO—Alternative Host Materials for Li^+ -Conducting Solid Polymer Electrolytes. *Prog. Polym. Sci.* **2018**, *81*, 114−143.

https://doi.org/10.1021/acspolymersau.3c00035
ACS Polym. Au 2024, 4, 77−85